Muonium Emission into Vacuum from Mesoporous Thin Films at Cryogenic Temperatures

A. Antognini,[1,*] P. Crivelli,[1,†] T. Prokscha,[2,‡] K. S. Khaw,[1] B. Barbiellini,[3] L. Liszkay,[4] K. Kirch,[1,2] K. Kwuida,[1] E. Morenzoni,[2] F. M. Piegsa,[1] Z. Salman,[2] and A. Suter[2]

[1]*Institute for Particle Physics, ETH Zurich, Switzerland*
[2]*Paul Scherrer Institute, Villigen, Switzerland*
[3]*Department of Physics, Northeastern University, Boston, Massachusetts 02115, USA*
[4]*CEA, Irfu, Sédi, Centre de Saclay, F-91191 Gif-sur-Yvette, France*

(Received 23 December 2011; published 3 April 2012)

We report on muonium (Mu) emission into vacuum following μ^+ implantation in mesoporous thin SiO_2 films. We obtain a yield of Mu into vacuum of $(38 \pm 4)\%$ at 250 K and $(20 \pm 4)\%$ at 100 K for 5 keV μ^+ implantation energy. From the implantation energy dependence of the Mu vacuum yield we determine the Mu diffusion constants in these films: $D_{\mathrm{Mu}}^{250\,\mathrm{K}} = (1.6 \pm 0.1) \times 10^{-4}\ \mathrm{cm}^2/\mathrm{s}$ and $D_{\mathrm{Mu}}^{100\,\mathrm{K}} = (4.2 \pm 0.5) \times 10^{-5}\ \mathrm{cm}^2/\mathrm{s}$. Describing the diffusion process as quantum mechanical tunneling from pore to pore, we reproduce the measured temperature dependence $\sim T^{3/2}$ of the diffusion constant. We extract a potential barrier of (-0.3 ± 0.1) eV which is consistent with our computed Mu work function in SiO_2 of $[-0.3, -0.9]$ eV. The high Mu vacuum yield, even at low temperatures, represents an important step toward next generation Mu spectroscopy experiments.

DOI: 10.1103/PhysRevLett.108.143401 PACS numbers: 36.10.Ee, 12.20.−m, 73.30.+y, 76.75.+i

Muonium (Mu), the bound state of a positive muon (μ^+) and an electron, is a purely leptonic atom. It is thus an ideal object for testing bound-state quantum electrodynamics (QED) free from hadronic uncertainties related to the structure of the nucleus [1,2]. The hyperfine splitting [3] and the $1S$-$2S$ transition frequency measurements of Mu [4,5] provide the best determination of the muon mass, of the muon magnetic moment, and of the charge ratio between muon and electron. The latter is the best verification of charge equivalence between the first two families of particles. Mu can also be used to search for new physics such as lepton flavor violation via muonium-antimuonium oscillation [6].

A renewed interest in this simple system has been triggered by the recent results of the muonic hydrogen experiment [7]. The study of nonbaryonic atoms, like muonium and positronium, may help to shed some light on the puzzling proton radius discrepancy observed between this measurement and the values obtained from hydrogen [8] and electron scattering experiments [9].

The quality of the Mu source was a main limitation in the measurements with muonium mentioned above (see, e.g., [1]). Therefore, for next generation experiments, it is essential to have a source of Mu with a high vacuum yield down to low temperature and long term stability. Mu in vacuum is typically produced by stopping a low momentum μ^+ beam close to the surface of tungsten foils [10] or silica powders [11]. The fraction of Mu which diffuses to the surface is emitted into vacuum. Prior to this study, the highest measured vacuum yield was $(18 \pm 2)\%$ per stopped μ^+ obtained in SiO_2 powders at 300 K [11–13]. Moreover, to our knowledge, Mu emission into vacuum below room temperature has never been reported. A Mu source with a larger flux can be achieved either by improving the μ^+ beam (smaller phase space, low energy, high intensity) as proposed in [14,15] or by improving the $\mu^+ \rightarrow$ Mu conversion. In this work, we focus on the optimization of the latter using SiO_2 porous films (F samples of [16]) which we preselected with the ETH Zurich slow positron beam. The choice of this material was motivated by the fact that positronium (Ps, the electron-positron bound state) and Mu share similar formation mechanisms. Recently, a yield of Ps into vacuum as high as 40% from these porous samples has been measured down to cryogenic temperatures [16]. In contrast to SiO_2 powders, those samples can be produced under well-controlled conditions with uniform pore sizes and distributions. The long term stability was measured with Ps for which the vacuum yield was constant in a time scale of months.

For this study, we used the low energy positive muon beam (LEM) at PSI delivering approximately 3000 s^{-1} μ^+ on target with energies tunable from 1 to 30 keV [17,18]. The μ^+ are implanted in the porous film of 1 μm thickness, a pore size of (5 ± 0.5) nm, and a density of 1.1 $\mathrm{g/cm}^3$. The mean implantation depth is 75(270) nm for a μ^+ implantation energy of 5(19) keV. The Mu formation mechanism is similar to the one in SiO_2 powders [11,19]. The μ^+ implanted at keV energy in the SiO_2 film rapidly thermalize in the bulk (in tens of ps). A fraction of them forms Mu in the bulk. Those atoms diffuse until they are ejected in the pores with almost 100% probability [11]. The porous films have a network of interconnected pores in which Mu can diffuse and lose its energy via collisions with the pore walls. If Mu reaches the film surface before decaying, it is emitted into vacuum. We define the Mu

vacuum yield as the probability of Mu emission into vacuum per implanted μ^+. If Mu suffered a sufficient number of collisions, during its diffusion to the surface, it becomes thermalized at the film temperature. While Ps from similar films is emitted into vacuum with an energy above room temperature [16,20] due to quantum mechanical confinement in the pores, for Mu one does not expect such a limitation because the de Broglie wavelength is about 10 times smaller, i.e., of the order of 0.4 nm.

The LEM is a dedicated facility for μSR (muon spin rotation) measurements. A sketch of the sample region and the positron detectors is shown in Fig. 1 (see [17,18] for more details). Before stopping in the sample, the μ^+, which are almost 100% transversely polarized, cross a 10 nm thin carbon foil causing the emission of secondary electrons. These electrons, detected by a microchannel plate, provide the event trigger. Segmented plastic scintillators surrounding the sample region in a cylindrical geometry are used to detect the positron from muon decay. The positron signal provides the stop time of the event. The sample resides in a magnetic field transverse to the muon spin (see Fig. 1). Therefore, the muon spin undergoes Larmor precession whose frequency depends on the local magnetic field and on whether the muon remains a free μ^+ or binds with an electron to form Mu. Since the positron from muon decay is emitted preferentially along the muon spin, using a segmented detector divided in four sections (top, bottom, left, right), it is possible to track the spin precession. The time spectra measured in each individual segment follow the exponential muon decay distribution, modulated at the Larmor frequency. The number of counts $N(t)$ measured in one of the positron detectors, e.g., upstream top, is [11]

$$N(t) = N_0 e^{-t/\tau}[1 + A_\mu(t) + A_{\mathrm{Mu}}(t)] + B,$$

where N_0 is the normalization, $\tau = 2.2\ \mu$s is the muon lifetime, B the uncorrelated background,

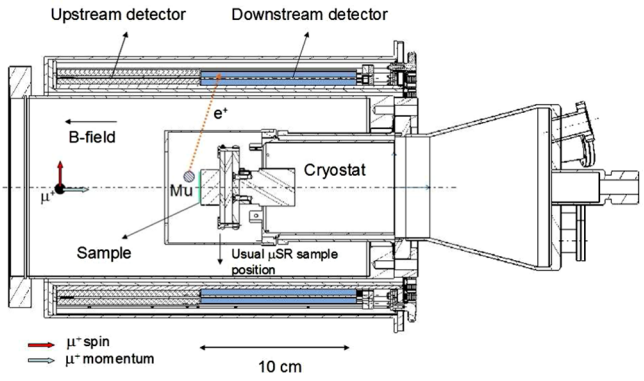

FIG. 1 (color online). LEM sample chamber. The sample is glued on a silver coated copper mount contacted to a cryostat. The sample is surrounded by scintillators for positron detection grouped in upstream and downstream counters. Each of them is additionally segmented in top, bottom, left, and right detectors.

$A_\mu(t) = A_\mu e^{-\lambda_\mu t}\cos(\omega_\mu t - \phi_\mu)$ and $A_{\mathrm{Mu}}(t) = A_{\mathrm{Mu}} e^{-\lambda_{\mathrm{Mu}} t}\cos(\omega_{\mathrm{Mu}} t - \phi_{\mathrm{Mu}})$ are the precession signals at frequencies ω_μ for free μ^+ and ω_{Mu} for Mu and phases ϕ_μ and ϕ_{Mu}. The constants λ_μ and λ_{Mu} take into account the damping of the precession signal amplitudes A_μ and A_{Mu} due to spin relaxation processes [19]. Since the gyromagnetic factor of Mu in the triplet state ($F = 1, M = \pm 1$) is 103 times larger than the gyromagnetic factor of μ^+ ($\omega_{\mathrm{Mu}} \approx 103\omega_{\mu^+}$), it is possible to clearly distinguish if an implanted μ^+ remains unbound or forms Mu.

The initial fraction of Mu formed in the sample per implanted μ^+ is determined with $F^0_{\mathrm{Mu}} = 1 - A_\mu/A_{\mathrm{tot}}$ where A_{tot} is the total observable asymmetry (the asymmetry at the time $t = 0$ when the μ^+ are implanted into the sample). The correctness of this indirect approach relies on the fact that μ^+ is not expected to depolarize in silica [21], and thus the missing μ^+ fraction is the one that converted to Mu. The measured Mu formation probability (see Fig. 2) for porous SiO_2 is $F^0_{\mathrm{Mu}} = (60 \pm 2)\%$ which is comparable with the results obtained in silica powders [11]. For Suprasil (fused quartz) we obtained $F^0_{\mathrm{Mu}} = (80 \pm 4)\%$ in agreement with [22]. In the same plot, we show the initial fraction of Mu extracted directly using $F^0_{\mathrm{Mu}} = 2A_{\mathrm{Mu}}/A_{\mathrm{tot}}$ [11]. As one can see, these values differ from the ones obtained indirectly from A_μ. Such an effect was already reported in [21] where it was attributed to the fact that the direct method is sensitive only to the fraction of Mu that does not undergo fast relaxation, e.g., due to spin exchange collisions in the pores.

Using the standard μSR setup allows us to determine the probability to form Mu. However, with this technique we are unable to demonstrate Mu emission into vacuum. One possibility would be to use a tracking detector as in [12]. We developed a new approach which exploits the existing

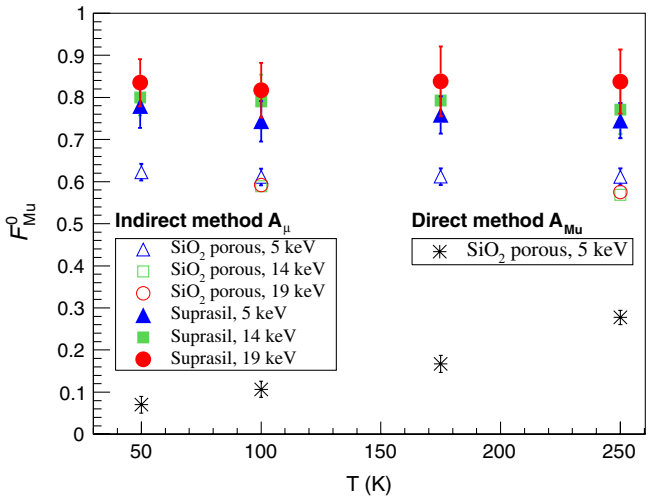

FIG. 2 (color online). F^0_{Mu} versus temperature for the porous film (8×10^6 events) and Suprasil (2.5×10^6 events) for various implantation energies obtained from the μSR amplitudes A_μ and A_{Mu}.

μSR setup. The principle is based on the fact that the detection efficiency in the downstream detectors (see Fig. 1) is time dependent in the case of Mu emission into vacuum. Positrons from Mu decaying outside of the film have a higher probability to be detected in the downstream counters than the ones coming from μ^+/Mu decays in the sample, which are shielded by the copper sample support. Therefore, if vacuum emission occurs, a deviation from the μ^+ exponential decay distribution is expected. Hereafter, we will refer to this method as the positron shielding technique (PST). Note that in PST we do not consider top, bottom, left, and right counters separately as in the μSR setup, but we only distinguish between upstream and downstream detectors. In Fig. 3(a), we show the time spectra expected in the downstream counters from simulations using GEANT4[23] for 0% (f_0) and 100% (f_{100}) Mu yield in vacuum. In Fig. 3(b), we present the measured data for Suprasil (no emission into vacuum, thus corresponding to 0%) and for SiO_2 porous material where emission into vacuum is expected. In order to determine the fraction of Mu emission into vacuum (F_v^{Mu}), we fit the measured time spectra with

$$f_{\mathrm{fit}}(t) = n[(1 - F^v_{\mathrm{Mu}})f_0(t) + F^v_{\mathrm{Mu}} f_{100}(t)] + n_{pp} f_{pp}(t),$$

where n is the normalization and $n_{pp}f_{pp}(t)$ accounts for a prompt peak. This prompt peak, which occurs in the first bins of the time spectra [see inset of Fig. 3(c)], originates from μ^+ decaying in flight before reaching the target and from backscattered μ^+ [24]. The time distribution of this peak $f_{pp}(t)$ is determined experimentally using the Suprasil sample. The three free parameters of the fit are n, n_{pp}, and F^v_{Mu}. Fits of $f_{\mathrm{fit}}(t)$ to the experimental data which have been taken for various implantation energies and film temperatures typically give a reduced χ^2 of 1.1–1.4 (612 degrees of freedom). In the simulations, Mu is assumed to be emitted from the surface of the sample with a $\cos\theta$ angular distribution [13,20] and an energy spectrum corresponding to a Maxwell-Boltzmann distribution at the target temperature. Fitting the data with an isotropic angular distribution or a different temperature worsens the reduced χ^2 by more than 0.2.

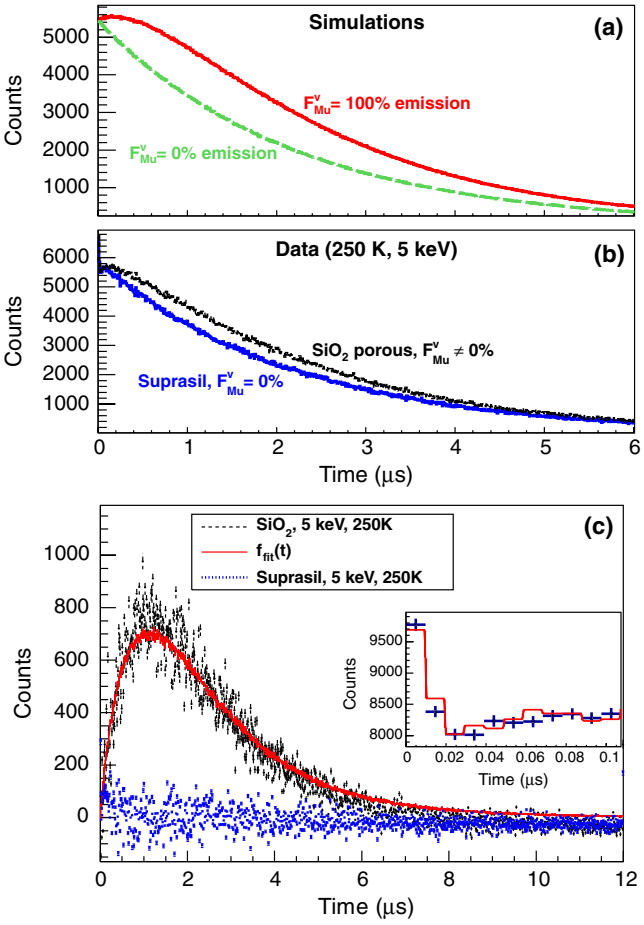

FIG. 3 (color online). (a) Simulated time distributions in the downstream detector for 0% (dashed green) and 100% (solid red). (b) Measured time spectra for the porous material (dotted black) and the Suprasil sample (solid blue). (c) Data and $f_{\mathrm{fit}}(t)$ after subtraction of the properly normalized exponential muon decay distribution. The inset shows the prompt peak and $f_{\mathrm{fit}}(t)$ (without subtraction).

In order to better visualize the comparison between simulations and measurements, in Fig. 3(c), we show the time spectrum after subtraction of the prompt peak and the exponential muon decay distribution. The Suprasil data give a constant value as expected, due to the absence of Mu emission from this sample. On the contrary, for the porous film there is a clear signal caused by the increased positron detection efficiency when Mu is emitted into vacuum. The values of F^v_{Mu} extracted from the fits are presented in Fig. 4. We obtain a yield of Mu into vacuum of $F^v_{\mathrm{Mu}} = (38 \pm 4)$% at 250 K and $F^v_{\mathrm{Mu}} = (20 \pm 4)$% at 100 K for 5 keV implantation energy. The abrupt change of F^v_{Mu} visible between 75 and 100 K is due to the thermal absorption of Mu at the pore walls as already reported for silica powders [25,26]. For 20 K, F^v_{Mu} is compatible with zero. The linear dependence of $F^v_{\mathrm{Mu}} \propto T$ (between 100 and 250 K) is interesting since from a classical diffusion model a $T^{1/4}$ dependence is expected. For comparison in Fig. 4(a), we also present the fraction of polarized Mu determined directly from the measurement of the Mu asymmetry A_{Mu} with the μSR technique. As one can see, these points are systematically lower than F^v_{Mu} obtained with PST. This is because PST, in contrast to the μSR direct method, is also sensitive to the fraction of Mu that depolarizes fast. Nevertheless, both methods give consistent results in terms of dependence on the sample temperature and μ^+ implantation energy (E).

In Fig. 4(b), F^v_{Mu} versus E at 100 and 250 K is fitted with a one-dimensional diffusion model originally developed for Ps [27,28]. The Mu fraction diffusing into vacuum is given by $F^v_{\mathrm{Mu}}(E) = F^0_{\mathrm{Mu}}(E)J(E)$ with $J(E) = \int_0^l e^{-\beta x} P(x, E)dx$, where l is the film thickness,

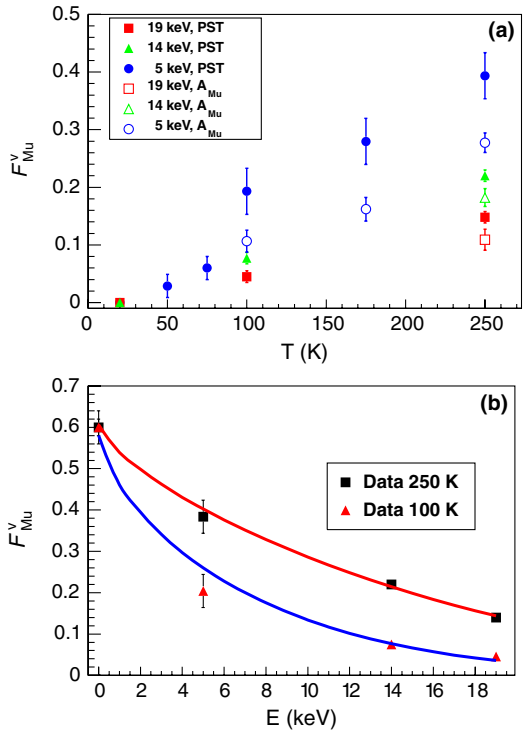

FIG. 4 (color online). (a) Vacuum yield F^v_{Mu} versus temperature determined with PST. For comparison, we show the results of the direct method. (b) F^v_{Mu} versus the implantation energy. The curves are fit with the diffusion model described in the text.

$\beta = 1/\sqrt{D_{\mathrm{Mu}}\tau}$ is the inverse of the diffusion length, and D_{Mu} is the diffusion coefficient. For the initial Mu fraction F^0_{Mu}, we used the value of 60% as obtained with the μSR indirect method (see Fig. 2). The μ^+ implantation profile $P(x, E)$ was calculated using the TRIMSP simulation validated for μ^+ with experimental data [29]. The only fit parameter to the data is the Mu diffusion constant D_{Mu}. The resulting values determined from the fits [solid lines in Fig. 4(b)] are $D^{250\,\mathrm{K}}_{\mathrm{Mu}} = (1.6 \pm 0.1) \times 10^{-4}$ cm^2/s and $D^{100\,\mathrm{K}}_{\mathrm{Mu}} = (4.2 \pm 0.5) \times 10^{-5}$ cm^2/s. The good agreement between fit and data implies that D_{Mu} does not depend on the implantation energy. This means that the Mu thermalization time is much shorter than the diffusion time (cf. this result with similar measurements in Ps, see Fig. 10 of [20]). A further argument that Mu quickly thermalizes is given by the worsening of the χ^2 when fitting the data of Fig. 3(c) with distributions simulated at temperatures different from the sample temperature. Therefore, we can write the diffusion coefficient as a function of the mean kinetic energy E_{Mu} of thermalized Mu in the pores as $D_{\mathrm{Mu}} = \Lambda/(3C) \times \sqrt{2E_{\mathrm{Mu}}/m_{\mathrm{Mu}}}$ where C is the mean number of collisions that Mu undergoes in one pore before reaching the next one, m_{Mu} is the Mu mass, and Λ is the mean distance between the pores [20]. Assuming an hexagonal close packing of the pores, one can estimate the mean separation between them using $\rho = \rho_0(1 - \pi d^3/\Lambda^3\sqrt{18})$ [20]. We obtain $\Lambda = 5.6$ nm for a pore diameter of $d = 5$ nm, a silica bulk density of $\rho_0 = 2.2$ g/cm^3, and a porous film density of $\rho = 1.1$ g/cm^3. Using the experimentally determined D_{Mu}, the mean number of collisions in each pore is $C = 2100 \pm 500$ at 100 K and $C = 850 \pm 100$ at 250 K. These values confirm that Mu thermalization is fast ($\sim$ ns) on the time scale of the diffusion process ($\sim$ μs). In fact, from the mass difference of Mu and SiO_2 [30], one expects that in order to reach thermal energy Mu needs $\sim$500 collisions.

The obtained D_{Mu} values are 3 orders of magnitude smaller than expected from a classical diffusion model [11]. In order to explain this disagreement, we interpret the Mu diffusion process in the porous material as quantum mechanical tunneling from pore to pore through a step potential barrier of (0.6 ± 0.2) nm width (corresponding to the pore walls thickness). From the mean number of collisions C, which is the inverse of the pore-to-pore tunneling probability, we deduce a height of the potential barrier of (0.3 ± 0.1) eV. The uncertainty is dominated by our poor knowledge of the material structure. With this quantum mechanical model we can reproduce the observed dependence of $D_{\mathrm{Mu}}(T)$ versus the temperature T. Since, in our regime, the tunneling probability scales approximately linearly with T, we obtain that $D_{\mathrm{Mu}}(T) \propto \sqrt{E_{\mathrm{Mu}}}/C \propto \sqrt{T}/T^{-1} \propto T^{3/2}$. The measured ratio $D^{250\,\mathrm{K}}_{\mathrm{Mu}}/D^{100\,\mathrm{K}}_{\mathrm{Mu}} \approx 3.8 \pm 0.5$ compares well with the expected value from the $T^{3/2}$ dependence of $(250\ \mathrm{K}/100\ \mathrm{K})^{3/2} \approx 4$, supporting the validity of our model. To check if the value of the potential barrier height obtained above can be identified with the Mu work function (W), we perform density functional theory calculations within GAUSSIAN 98 [31] on clusters of SiO_2 containing up to eight silicon atoms and terminated by oxygen, capped with hydrogen atoms. We compute the total energy $E^{\mathrm{tot}}_{\mathrm{SiO_2+Mu}}$ of the SiO_2 matrix with a Mu atom and the total energy of the SiO_2 fragment alone $E^{\mathrm{tot}}_{\mathrm{SiO_2}}$. These computations of $W = E^{\mathrm{tot}}_{\mathrm{SiO_2+Mu}} - E^{\mathrm{tot}}_{\mathrm{SiO_2}} - 13.6$ eV yield a value between -0.3 and -0.9 eV. This interval for W originates from the uncertainty to locate the exact position of the interstitial Mu site with respect the Si and O atoms. Considering the oversimplification of our model, we conclude that our experimental determination of the work function is consistent with the theoretical estimation. Further experiments using other techniques and more precise measurements for Mu and Ps will be useful to gain a deeper understanding of this intriguing diffusion process in mesoporous films.

Summarizing, we have found that a sizeable fraction of thermalized muonium is emitted into vacuum from mesoporous thin SiO_2 films. At 250 K the yield is more than a factor of 2 higher than previously found in SiO_2 powders at room temperature and comparable at 100 K. The high muonium yield, even at low temperatures, is an important step toward the development of low emittance Mu sources for spectroscopy experiments. We are aiming to measure

the 1*S*-2*S* energy interval of muonium. Our source of cold Mu opens the possibility of performing continuous wave laser spectroscopy of this transition. This decreases both statistical and systematical uncertainties compared to the previous experiment since the power broadening and residual first order Doppler shift related to the pulsed laser will be eliminated. With a muon beam similar to the one used for this measurement, an improvement of more than an order of magnitude can be achieved resulting in the best determination of the muon mass and providing an improved check of bound-state QED calculations.

This work was supported in part by the SNSF under the Ambizione Grant No. PZ00P2_132059, the SNSF Grant No. 200021-129600 and the DOE Contract No. DE-FG02-07ER46352. We thank A. Badertscher, U. Gendotti, F. Kottmann, G. Marshall, A. Rubbia, R. Scheuermann, D. Taqqu, the PSI and ETH workshops, the ETH Labortechnik group of H. Scherrer, the PSI accelerator group, and the NERSC and NU-ASCC computation centers.

*aldo@phys.ethz.ch
†crivelli@phys.ethz.ch
‡thomas.prokscha@psi.ch

[1] K. Jungmann, Nucl. Phys. **B155**, 355 (2006).
[2] S. G. Karshenboim, Phys. Rep. **422**, 1 (2005).
[3] W. Liu *et al.*, Phys. Rev. Lett. **82**, 711 (1999).
[4] S. Chu, A. P. Mills, A. G. Yodh, K. Nagamine, Y. Miyake, and T. Kuga, Phys. Rev. Lett. **60**, 101 (1988).
[5] V. Meyer *et al.*, Phys. Rev. Lett. **84**, 1136 (2000).
[6] L. Willmann *et al.*, Phys. Rev. Lett. **82**, 49 (1999).
[7] R. Pohl *et al.*, Nature (London) **466**, 213 (2010).
[8] P. J. Mohr, B. N. Taylor, and D. B. Newell, Rev. Mod. Phys. **80**, 633 (2008).
[9] I. Sick, Phys. Lett. B **576**, 62 (2003).J. C. Bernauer *et al.*, Phys. Rev. Lett. **105**, 242001 (2010); X. Zhan *et al.*, Phys. Lett. B **705**, 59 (2011).
[10] A. P. Mills, J. Imazato, S. Saitoh, A. Uedono, Y. Kawashima, and K. Nagamine, Phys. Rev. Lett. **56**, 1463 (1986).
[11] G. M. Marshall, J. B. Warren, D. M. Garner, G. S. Clark, J. H. Brewer, and D. G. Fleming, Phys. Lett. **65A**, 351 (1978).
[12] G. A. Beer *et al.*, Phys. Rev. Lett. **57**, 671 (1986).
[13] A. C. Janissen *et al.*, Phys. Rev. A **42**, 161 (1990).
[14] A. Toyoda *et al.*, arXiv:1110.1125.
[15] D. Taqqu, Phys. Rev. Lett. **97**, 194801 (2006).
[16] P. Crivelli, U. Gendotti, A. Rubbia, L. Liszkay, P. Perez, and C. Corbel, Phys. Rev. A **81**, 052703 (2010).
[17] E. Morenzoni *et al.*, Physica B (Amsterdam) **289–290**, 653 (2000).
[18] T. Prokscha, E. Morenzoni, K. Deiters, F. Foroughi, D. George, R. Kobler, A. Suter, and V. Vrankovic, Nucl. Instrum. Methods Phys. Res., Sect. A **595**, 317 (2008).
[19] R. F. Kiefl, J. B. Warren, C. J. Oram, G. M. Marshall, J. H. Brewer, D. R. Harshman, and C. W. Clawson, Phys. Rev. B **26**, 2432 (1982).
[20] D. B. Cassidy, P. Crivelli, T. H. Hisakado, L. Liszkay, V. E. Meligne, P. Perez, H. W. K. Tom, and A. P. Mills, Phys. Rev. A **81**, 012715 (2010).
[21] K. A. Woodle, Z. Phys. D **9**, 59 (1988).
[22] T. Prokscha, E. Morenzoni, D. G. Eshchenko, N. Garifianov, H. Glückler, R. Khasanov, H. Luetkens, and A. Suter, Phys. Rev. Lett. **98**, 227401 (2007).
[23] S. Agostinelli *et al.*, Nucl. Instrum. Methods Phys. Res., Sect. A **506**, 250 (2003).
[24] T. Paraiso, E. Morenzoni, T. Prokscha, and A. Suter, Physica B (Amsterdam) **374–375**, 498 (2006).
[25] R. F. Kiefl, B. D. Patterson, E. Holzschuh, W. Odermatt, and D. R. Harshman, Hyperfine Interact. **18**, 563 (1984).
[26] D. R. Harshmann, R. Keitel, M. Senba, R. F. Kiefl, E. J. Ansaldo, and J. H. Brewer, Phys. Lett. **104A**, 472 (1984).
[27] K. G. Lynn and H. Lutz, Phys. Rev. B **22**, 4143 (1980).
[28] J. Xu, J. Moxom, S. Yang, R. Suzuki, and T. Ohdaira, Chem. Phys. Lett. **364**, 309 (2002).
[29] E. Morenzoni, H. Glückler, T. Prokscha, R. Khasanov, H. Luetkens, M. Birke, E. M. Forgan, Ch. Niedermayer, and M. Pleines, Nucl. Instrum. Methods Phys. Res., Sect. B **192**, 254 (2002).
[30] G. W. Ford, L. M. Sander, and T. A. Witten, Phys. Rev. Lett. **36**, 1269 (1976).
[31] M. J. Frisch *et al.*, GAUSSIAN 98 (Gaussian, Inc., Pittsburgh, 1998).